JOURNAL OF CATALYSIS **169,** 45–54 (1997)
ARTICLE NO. CA971686

Kinetics and Mechanism of the Reduction of NO by C_3H_8 over Pt/Al_2O_3 under Lean-Burn Conditions

R. Burch[1] and T. C. Watling

Catalysis Research Centre, Chemistry Department, University of Reading, Whiteknights, Reading RG6 6AD, United Kingdom

Received November 7, 1996; revised February 28, 1997; accepted February 28, 1997

The effect of temperature, contact time, and reactant concentration on the kinetics of NO reduction by C_3H_8 under lean burn conditions over Pt/Al_2O_3 has been investigated and a kinetic model which satisfactorily fits the data has been developed. Under reaction conditions adsorbed atomic oxygen is the dominant species on the metal surface, resulting in C_3H_8 oxidation being inhibited by O_2 and in the facile oxidation of NO to NO_2. The rate determining step in C_3H_8 oxidation by O_2 is believed to be dissociative chemisorption of C_3H_8 involving the breaking of a C–H bond. Possible mechanisms for the reduction of NO to N_2 and N_2O are discussed and the kinetics predicted for each mechanism, compared with the empirical data. It is concluded that NO dissociation on the Pt surface is not a major route. Instead, the reduction of NO appears to occur by spillover of NO_2 from the Pt metal onto the Al_2O_3 support where it reacts with C_3H_8-derived species to form N_2 and N_2O.

INTRODUCTION

There is currently much interest in the catalytic reduction of NO_x in the presence of excess O_2, as demonstrated by the recent reviews on the subject (1, 2). One promising catalyst system is based on platinium group metals supported on metal oxides. These catalysts have been shown to be durable in real diesel exhaust and are resistant to poisoning by SO_2 (3, 4).

Despite the level of interest there have been no detailed investigations published concerning the reaction kinetics of NO_x reduction over these catalysts under lean burn conditions. Kinetics studies are important as they may give insight into the mechanism of the reaction, which in turn aids the understanding of how better catalysts might be designed. Knowledge of the kinetics and mechanism are also required for the development of kinetic models which are required for modelling the behaviour of real exhaust catalysts.

In this paper, we report a kinetics study of the lean deNO_x reaction over Pt/Al_2O_3 using C_3H_8 as the reductant. The effect of temperature, contact time, and reactant composition on the reaction have been investigated. From this information a realistic reaction mechanism has been proposed, and from this a kinetic model has been developed which satisfactorily predicts the observed kinetics. However, it should be noted that while the reaction mechanism proposed here is consistent with the empirical kinetics this does not constitute a final proof of the proposed mechanism, although evidence from the literature to support this mechanism is presented.

[1] Corresponding author. E-mail: R.Burch@reading.ac.uk.

EXPERIMENTAL

The platinum on γ-alumina catalyst used in this study was prepared by incipient wetness impregnation using dinitrodiammine-Pt as the precursor. The sample was calcined at 500°C for 14 h and had a 1 wt% Pt loading, a dispersion of 69% (by H_2 chemisorption) and a grain size of 250–850 μm.

Catalyst testing was carried out using a quartz tubular downflow reactor (I.D. 5 mm). The sample (100 mg) was held between plugs of quartz wool. Reactant gases were fed from independent mass flow controllers. Unless stated otherwise the feed consisted of 1000 ppm C_3H_8, 1000 ppm NO, and 5% O_2 in He and the total flow was 200 cm^3 min^{-1} (corresponding to a space velocity of 87,000 h^{-1}). The reactor outflow was analysed using a Perkin Elmer Autosystem gas chromatograph with a TCD detector, a Signal Series 2000 IR CO_2 analyser and a Signal Series 4000 chemiluminescence NO_x analyser (for NO and total NO_x (i.e., $NO + NO_2$)). The chromatograph used a Heysep N column for the separation of CO_2, N_2O, C_3H_8, and H_2O, and a molecular sieve 13X column for the separation of O_2, N_2, and CO, as described in more detail elsewhere (5). No reaction was observed over quartz wool, provided the temperature was below 600°C. Changing the catalyst grain size had no effect on the conversions, indicating freedom from intraparticle transport limitation.

For experiments in which the temperature was varied, the temperature was increased stepwise with constant feed composition and total flow. For determining the effect of contact time, measurements were made at a series of total flows between 50–200 cm^3 min^{-1}. The flow was varied in

0021-9517/97 $25.00

a random way rather than sequentially, to avoid any bias in the data. Similarly, for determining the effect of reactant concentration, the concentration of one reactant was varied in a nonsequential manner, while the concentration of the other reactants were kept constant.

RESULTS

The effect of temperature on the C_3H_8–NO–O_2 reaction over 1% Pt/Al_2O_3 is shown in Fig. 1. Significant C_3H_8 conversion starts at about 230°C. Conversion of NO to NO_2 was observed from temperatures above 170°C. This contrasts with the C_3H_6–NO–O_2 (6, 7) reaction in which NO_2 is only formed after complete conversion of the hydrocarbon has occurred. The maximum conversion of NO to NO_2 was 35% and occurred at 290°C. The maximum NO_x conversion was 25% occurring at 430°C. Unlike the C_3H_6–NO–O_2 reaction (6–8), the maximum NO_x conversion occurs before total hydrocarbon conversion is reached. The selectivity to N_2 ignoring NO_2 production, S_{N_2}, was about 60% at temperatures between 310 and 370°C, but appears to increase at higher temperatures (>400°C).

The effect of contact time (reciprocal space velocity) on the C_3H_8–NO–O_2 reaction at 310°C is given in Fig. 2. The conversions of C_3H_8 and of NO to N_2 and N_2O were both linear in contact time, indicating that the reactor was behaving differentially and that the reaction was free from interparticle transport limitation. The conversion of NO to NO_2 was independent of contact time, suggesting that the rate of NO oxidation to NO_2 is so fast that a pseudo-equilibrium was established between NO and NO_2 even at the shortest contact time used. Engler *et al.* (8) have also reported the conversion of NO to NO_2 to be independent of contact time in the *n*-$C_{16}H_{34}$–NO–O_2 reaction over supported Pt. The ratio of N_2 : N_2O formed is subject to relatively large errors due to the low sensitivity of the GC TCD to these components. The average ratio of N_2 : N_2O formed was about 2 : 1.

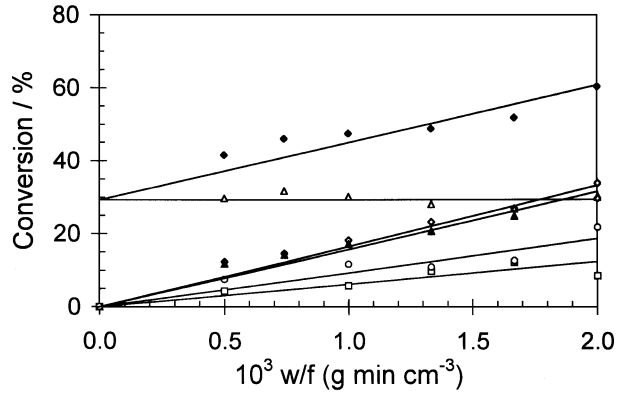

FIG. 2. The effect of varying the reciprocal space velocity, w/f, on the C_3H_8–NO–O_2 reaction at 310°C over 100 mg of 1% Pt/Al_2O_3. Feed: 1000 ppm C_3H_8, 1000 ppm NO, and 5% O_2 (◇, C_3H_8; ◆, NO; ▲, NO_x; ○, NO to N_2; □, NO to N_2O; △, NO to NO_2).

Figure 3 shows the effect of C_3H_8 concentration on the C_3H_8–NO–O_2 reaction at 310°C. In this figure the production of NO_2 has been expressed as a conversion, since NO and NO_2 are in a pseudo-equilibrium (see above) and therefore it is not meaningful to use a turnover frequency (TOF) for this reaction. The rates of the other reactions have been expressed as TOFs. The rates of conversion of NO to N_2O and N_2, (and, hence, of total NO_x removal) were independent of C_3H_8 concentration. The conversion of NO to NO_2 decreased with increasing C_3H_8 concentration. The rate of C_3H_8 consumption was first order with respect to C_3H_8 if points between 200 and 2000 ppm C_3H_8 are considered, or greater than first order if all points are used. Similarly, Yao (9) has reported the order in C_3H_8 to be as high as 2 for oxidation of C_3H_8 by O_2 over Pt/Al_2O_3.

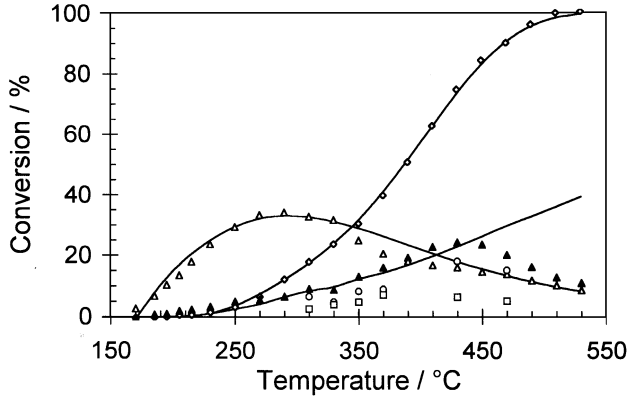

FIG. 1. The effect of varying temperature on the C_3H_8–NO–O_2 reaction over 100 mg of 1% Pt/Al_2O_3. Feed: 1000 ppm C_3H_8, 1000 ppm NO, and 5% O_2. Total flow 200 cm^3 min^{-1}. Lines are fit to kinetic model (◇, C_3H_8; ▲, NO_x; ○, NO to N_2; □, NO to N_2O; △, NO to NO_2).

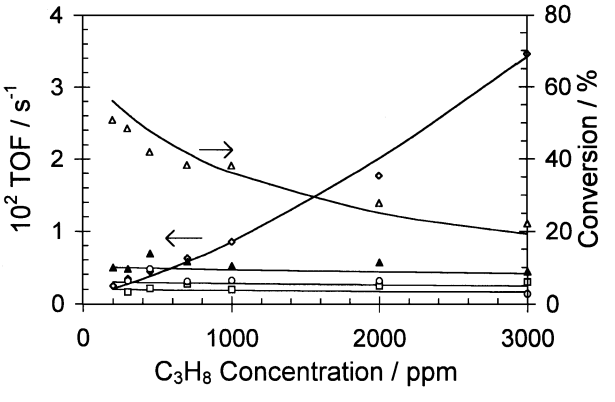

FIG. 3. The effect of varying C_3H_8 concentration on the TOF of C_3H_8 (◇), total NO_x (▲), NO to N_2 (○), and NO to N_2O (□), and on conversion of NO to NO_2 (△) for reaction at 310°C over 100 mg of 1% Pt/Al_2O_3. Feed: 1000 ppm NO and 5% O_2. Total flow 200 cm^3 min^{-1}. Lines are fit to kinetic model.

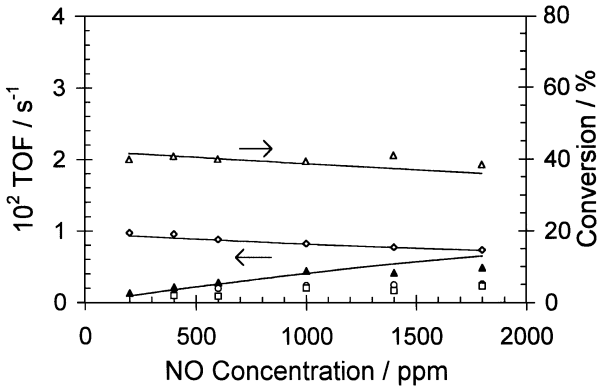

FIG. 4. The effect of varying NO concentration on the TOF of C_3H_8 (◇), total NO_x (▲), NO to N_2 (○), and NO to N_2O (□), and on conversion of NO to NO_2 (△) for reaction at 310°C over 100 mg of 1% Pt/Al_2O_3. Feed: 1000 ppm C_3H_8 and 5% O_2. Total flow 200 cm^3 min^{-1}. Lines are fit to kinetic model.

The effect of NO concentration on the C_3H_8–NO–O_2 reaction is shown in Fig. 4. The rate of C_3H_8 consumption decreases linearly with increasing NO concentration, i.e., NO inhibits the reaction of C_3H_8. Engler *et al.* (8) also report a linear decrease in alkane conversion with increasing NO concentration for the *n*-$C_{16}H_{34}$–NO–O_2 reaction over supported Pt. The conversion of NO to NO_2 was almost independent of NO concentration. The rate of NO_x removal increased with increasing NO concentration. Within experimental error, there was no significant change in the ratio of $N_2 : N_2O$ produced with NO concentration.

Figure 5 shows the effect of O_2 concentration on the C_3H_8–NO–O_2 reaction at 310°C. Increasing O_2 concentration initially results in a decrease in the rate of C_3H_8 consumption ($1 < [O_2] < 3\%$); i.e., C_3H_8 oxidation is inhibited by O_2, while at higher O_2 concentrations ($[O_2] > 5\%$) C_3H_8 conversion becomes independent of O_2 concentration. The conversion of NO to NO_2 increased nonlinearly with increasing O_2 concentration. The NO_x conversion initially increased with increasing O_2 concentration, but became independent of it for $[O_2] > 5\%$, i.e., at the same point as the rate of C_3H_8 consumption becomes zero order in O_2. Within experimental error, there was no significant change in the ratio of $N_2 : N_2O$ produced with O_2 concentration.

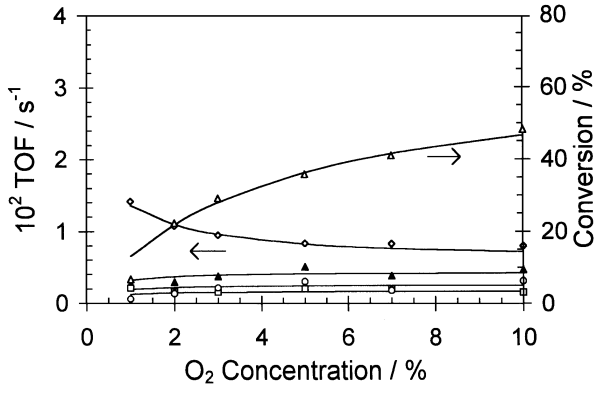

FIG. 5. The effect of varying O_2 concentration on the TOF of C_3H_8 (◇), total NO_x (▲), NO to N_2 (○), and NO to N_2O (□), and on conversion of NO to NO_2 (△) for reaction at 310°C over 100 mg of 1% Pt/Al_2O_3. Feed: 1000 ppm C_3H_8 and 1000 ppm NO. Total flow 200 cm^3 min^{-1}. Lines are fit to kinetic model.

DISCUSSION

The kinetics results have been interpreted in terms of a kinetic model which is developed below. The reactions occurring on the catalyst have been separated into the reaction of C_3H_8 with O_2, the conversion between NO and NO_2 and the deNO$_x$ reaction itself (i.e., the reaction of NO and/or NO_2 to form N_2 and N_2O). In this model it is assumed that all the sites on the Pt surface are equivalent and that there is no adsorbate–adsorbate interaction other than that due to chemical reaction. For convenience, the proposed reaction mechanism is summarised in Fig. 10.

Reaction of C_3H_8 with O_2 in the Presence of NO_x

C_3H_8 is a saturated molecule and therefore must break a bond to chemisorb on the Pt surface and react. In the literature the rate-determining step of alkane oxidation is generally reckoned to be dissociative chemisorption involving the breaking of a C–H bond (10). In our model the initial step involves the abstraction of a hydrogen (weakly acidic) from the propane by an adsorbed O atom (basic site) to give an adsorbed hydroxyl, with the resulting propyl species being bonded to a neighbouring, previously vacant site (Fig. 6). This is envisaged to occur via interaction between the partial negative charge on the adsorbed O and the partial positive charge on the hydrogen atom and the interaction between the partial positive charge on the vacant Pt with the partial negative charge on the carbon atom adjacent to the hydrogen atom. This can be expressed as

$$C_3H_{8(g)} + O* + * \rightarrow C_3H_7* + OH* \quad k_{C_3H_8} c_{C_3H_8} \theta_O \theta_V, \quad [1]$$

where θ_O and θ_V are the fractional coverages of oxygen and vacant sites, $c_{C_3H_8}$ is the concentration of C_3H_8, $k_{C_3H_8}$ is a rate constant, and $*$ represents a vacant site. Evidence for this heterolytic C–H bond breaking on a partially oxygen covered Pt surface is given in a recent review (10). Note that Eq. [1] predicts that the rate of C_3H_8 oxidation will be

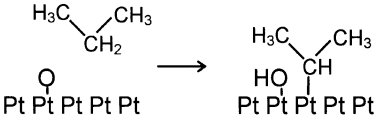

FIG. 6. Schematic representation of the rate determining step in C_3H_8 oxidation over a Pt catalyst. The active site consists of two adjacent sites, one of which has an adsorbed O atom on it and the other of which is vacant.

greatest when $\theta_O = \theta_V = 0.5$, which has been observed for the oxidation of CH_4 over Pt catalysts (11). This expression is also consistent with the order in C_3H_8 being greater than unity. Under the conditions used here, the reaction is inhibited by O_2, suggesting that $\theta_O > \theta_V$. As the C_3H_8 concentration is increased the rate of removal of adsorbed oxygen from the surface increases,[2] resulting in a fall in θ_O and a corresponding increase in θ_V. This changes the surface coverages towards that required for maximum activity resulting in an increase in the rate of C_3H_8 oxidation in addition to that due to the C_3H_8 term, in Eq. [1]; i.e., the order in C_3H_8 is greater than unity, as experimentally observed.

After the initial dissociative adsorption, the adsorbed propyl species reacts rapidly in a series of steps to give CO_2 and surface hydroxyls, which in turn rapidly react to give H_2O. If these steps were not rapid, then a significant coverage of C_3H_8-derived species and/or hydroxyl groups would build up on the surface, inhibiting the reaction and resulting in the order in C_3H_8 being less than unity. The rapid reaction of the propyl species is in part due to the high surface coverage of oxygen,

$$C_3H_7* + 13O* \rightarrow 3CO_{2(g)} + 7OH* + 7* \quad [2]$$

$$2OH* \rightarrow H_2O_{(g)} + O* + *. \quad [3]$$

Note that reaction [2] represents a series of reaction steps, rather than a single reaction step.

Oxygen presumably adsorbs dissociatively and irreversibly on the Pt surface; the desorption of adsorbed atomic oxygen is reported to occur only at temperatures above 400°C (12). The fact that the order in oxygen becomes zero order for $[O_2] > 5\%$ suggests that there are still vacant sites at which C_3H_8 molecules react, even though the oxygen coverage has reached saturation. This is reasonable, since, for example, CO can adsorb on an oxygen-saturated Pt surface (12). The dissociative adsorption of oxygen is assumed to occur in two steps. First, oxygen adsorbs reversibly and molecularly:

$$O_{2(g)} + * \rightleftharpoons O_2*, \quad K_{O_2} = \frac{\theta_{O_2}}{c_{O_2}\theta_V}. \quad [4]$$

This molecularly adsorbed oxygen then dissociates irreversibly. To allow for the saturation coverage of atomic oxygen being less than unity, the rate at which adsorbed O_2 dissociates is given by the product of the O_2 coverage and the vacant sites less $(1 - \theta_{O,MAX})$, where $\theta_{O,MAX}$ is the maximum coverage of oxygen,

$$O_2* + * \rightarrow 2O*, \quad k_O\theta_{O_2}(\theta_{O,MAX} - 1 + \theta_V). \quad [5]$$

This mechanism for oxygen adsorption has been confirmed by a recent TAP study of oxygen adsorption on Pt powder (13).

Finally, NO and NO_2 are presumed to adsorb molecularly and reversibly on the Pt surface,

$$NO_{(g)} + * \rightleftharpoons NO*, \quad K_{NO} = \frac{\theta_{NO}}{c_{NO}\theta_V}, \quad [6]$$

$$NO_{2(g)} + * \rightleftharpoons NO_2*, \quad K_{NO_2} = \frac{\theta_{NO_2}}{c_{NO_2}\theta_V}, \quad [7]$$

where K_{NO} and K_{NO_2} are the adsorption coefficients of NO and NO_2, respectively.

Using the steady state approximation for the coverage of oxygen for reactions [1]–[5] gives

$$2k_{OX}c_{O_2}\theta_V(\theta_{O,MAX} - 1 + \theta_V) = 10\,k_{C_3H_8}c_{C_3H_8}\theta_O\theta_V, \quad [8]$$

where $k_{OX} = k_O K_{O_2}$.

The number of surface sites is assumed to be constant; i.e.,

$$1 = \theta_V + \theta_O + \theta_{O_2} + \theta_{NO} + \theta_{NO_2}. \quad [9]$$

Combining Eqs. [6], [7], [8], and [9] and assuming θ_{O_2} to be negligible gives

$$\theta_V = \frac{k_{C_3H_8}c_{C_3H_8} + k_{OX}c_{O_2}(1 - \theta_{O,MAX})/5}{k_{C_3H_8}c_{C_3H_8}(1 + K_{NO}c_{NO} + K_{NO_2}c_{NO_2}) + k_{OX}c_{O_2}/5} \quad [10]$$

$$\theta_O = \frac{k_{OX}c_{O_2}(\theta_{O,MAX} - (K_{NO}c_{NO} + K_{NO_2}c_{NO_2})(1 - \theta_{O,MAX}))}{5(k_{C_3H_8}c_{C_3H_8}(1 + K_{NO}c_{NO} + K_{NO_2}c_{NO_2}) + k_{OX}c_{O_2}/5)}. \quad [11]$$

The derivation of Eqs. [10] and [11] are given in more detail in Appendix 1. Substituting Eqs. [10] and [11] into Eq. [1] gives an expression for the rate of C_3H_8 oxidation by O_2,

$$r_{C_3H_8-O_2} = \frac{k_{C_3H_8}c_{C_3H_8}k_{OX}c_{O_2}(k_{C_3H_8}c_{C_3H_8} + k_{OX}c_{O_2}(1 - \theta_{O,MAX})/5)(\theta_{O,MAX} - (K_{NO}c_{NO} + K_{NO_2}c_{NO_2})(1 - \theta_{O,MAX}))}{5\,(k_{C_3H_8}c_{C_3H_8}(1 + K_{NO}c_{NO} + K_{NO_2}c_{NO_2}) + k_{OX}c_{O_2}/5)^2}. \quad [12]$$

This expression fits the experimental data reasonably well (Figs. 3–5), using the parameters given in Table 1.

Conversion of NO to NO_2

The conversion of NO to NO_2 is independent of contact time (Fig. 2), indicating that NO_2 is being removed at the same rate as it is formed. However, the NO_2 concentration in not at thermodynamic equilibrium, since the conversion of NO to NO_2 (about 30%) is much less than that predicted

[2] As oxygen is irreversibly adsorbed (see below), adsorbed oxygen can only be removed by reaction.

TABLE 1

Parameters Obtained from Fitting Model to Experimental Data

Parameter	Value at 310°C	$E^{\ddagger}$/kJ mol^{-1} [a]	$\Delta H^{\ominus}$/kJ mol^{-1} [b]
k_{OX}	1.74×10^2 s^{-1} %$^{-1}$	119	—
$k_{C_3H_8}$	8.58×10^{-4} s^{-1} ppm^{-1}	62.8	—
$\theta_{O,MAX}$	0.994	—	—
K_{NO}	1.36×10^{-2} ppm^{-1}	—	−38.7
K_{NO_2}	1.35×10^{-2} ppm^{-1}	—	−38.7
k_{NO_x}	4.94×10^{-2} s^{-1}	101	—
$k_{NO_2,f}/k_{NO_2,b}$	7.93×10^{-5}	−72.3[c]	—
S_{N_2}	60%	—	—

[a] Activation energy for appropriate reaction step.
[b] Standard enthalpy of adsorption of appropriate species.
[c] Difference in activation energies of $k_{NO,f}$ and $k_{NO,b}$ ($E^{\ddagger}_{NO_2,f} - E^{\ddagger}_{NO_2,b}$).

for equilibrium in the presence of 5% O_2 at this temperature (79%). In addition, the fall in conversion to NO_2 with increasing C_3H_8 concentration (Fig. 3) is not predicted by thermodynamics. (This fall in conversion is not due to the reduction in O_2 concentration as a result of reaction with the increased amount of C_3H_8, since O_2 is present in such a large excess that its concentration is little affected by the amount of C_3H_8 converted.)

The interconversion between NO and NO_2 and the rates of NO_2 formation from NO and of NO_2 dissociation to give NO can be written as

$$NO_{(g)} + O* \rightarrow NO_2*, \quad k_{NO_2,f} c_{NO} \theta_O, \qquad [13]$$

$$NO_2* \rightarrow NO_{(g)} + O*, \quad k_{NO_2,b} \theta_{NO_2}, \qquad [14]$$

where $k_{NO_2,f}$ and $k_{NO_2,b}$ are rate constants for the forward and back reactions for NO_2 formation. If it is assumed that these reactions are much faster than any reaction of NO or NO_2 to give N_2 and N_2O (i.e., NO and NO_2 are in pseudo-equilibrium), application of the stationary state approximation to the NO_2 coverage and substitution of Eq. [7] gives the following expression for c_{NO_2} from which the conversion to NO_2 can be calculated:

$$c_{NO_2} = \frac{k_{NO_2,f} c_{NO} \theta_O}{K_{NO_2} k_{NO_2,b} \theta_V}. \qquad [15]$$

This expression fits the empirical data reasonably well (Figs. 3–5).

DeNO$_x$ Reaction

A number of models, based on mechanisms proposed in the literature, were tried for the deNO$_x$ reaction. Since the selectivity to N_2 and N_2O were little influenced by the reactant composition the rate of the deNO$_x$ reaction is proportional to the rate of NO dissociation and, hence, only the rate of this step needs to be considered. A number of the models tried are listed in Table 2, while Figs. 7–9 show the rate of NO_x removal calculated from these models. The curves in these figures where calculated in the same way as those in Figs. 3–5, i.e., assuming differential conditions. In all these models the ratio of selectivity to N_2 ignoring NO_2 formation was assumed to be 60% independent of reactant concentration.

One possibility suggested in the literature is that the reaction occurs between NO or NO_2 and C_3H_8 derived species on the metal surface. These reactions may involve nitrogen-containing organic compounds [14] or isocyanates [15] as intermediates on the metal surface. Carbonaceous species-assisted NO dissociation [5] is also included in this type of mechanism. The derivation of these models is given in Appendix 2. Gas phase reaction between NO or NO_2 and C_3H_8 was also considered (Table 2). However, none of these models fitted the empirical data (Figs. 7–9); e.g., none of these models predicted the rate of deNO$_x$ to be zero order in C_3H_8 concentration (Fig. 7). One of the reasons for this mechanism not being significant may be that the concentration of carbonaceous species on the metal surface is very low (see above).

Another possibility is that NO dissociation occurs on vacant Pt sites. In this case NO dissociation can be represented as

$$NO* + * \rightarrow N* + O*, \quad k_{NO_x} \theta_{NO} \theta_V = k_{NO_x} K_{NO} c_{NO} \theta_V^2. \qquad [16]$$

However, this expression did not fit the data (Figs. 7–9). This can be seen, for example, by considering the effect of O_2 concentration on the reaction rates (Fig. 5). As the O_2

TABLE 2

Models Considered for the Reaction of NO$_x$ to Form N_2 and N_2O

Number	Rate expression[a]	Mechanism of deNO$_x$
1	$k_{NO_x} r_{C_3H_8} \theta_{NO_2} / \theta_O$ [b]	NO_2 reacts with carbonaceous species (Type 1) on Pt
2	$k_{NO_x} r_{C_3H_8} \theta_{NO_2} / \theta_V$ [b]	NO_2 reacts with carbonaceous species (Type 2) on Pt
3	$k_{NO_x} r_{C_3H_8} \theta_{NO} / \theta_O$ [b]	NO reacts with carbonaceous species (Type 1) on Pt[c]
4	$k_{NO_x} r_{C_3H_8} \theta_{NO} / \theta_V$ [b]	NO reacts with carbonaceous species (Type 2) on Pt[c]
5	$k_{NO_x} c_{NO} c_{C_3H_8}$	Gas phase reaction between NO and C_3H_8
6	$k_{NO_x} c_{NO_2} c_{C_3H_8}$	Gas phase reaction between NO_2 and C_3H_8
7	$k_{NO_x} \theta_{NO} \theta_V$	Dissociation of NO on Pt
8	$k_{NO_x} \theta_{NO_2}$	Reaction of spillover NO_2 with carbonaceous species on Al_2O_3

[a] Rate equation for the rate of NO dissociation. Since selectivity to N_2 is little changed by the feed composition, this is proportional to rate of NO_x removal.
[b] $r_{C_3H_8}$ = calculated rate of C_3H_8 oxidation.
[c] This can be regarded as carbonaceous species assisted NO dissociation. It is also expression for reaction via organic nitrogen compounds or isocyanates on the Pt surface.

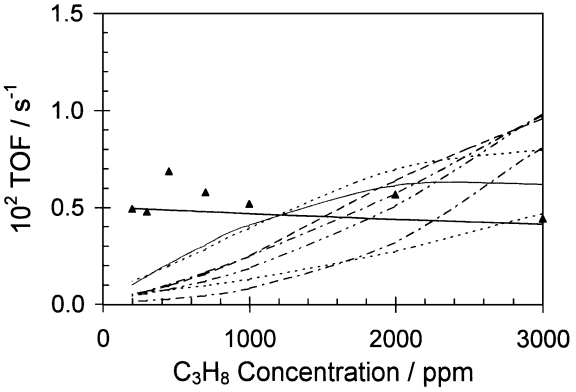

FIG. 7. Attempts at fitting various models to the experimental data for the effect of C_3H_8 concentration on the rate of deNO_x; ▲, experimental points. Lines are fits to models given in Table 2: from top to bottom at 1400 ppm C_3H_8, models 2, 6, 8, 1, 5, 4, 7, and 3; model 8 (the preferred model) is indicated by the bold line.

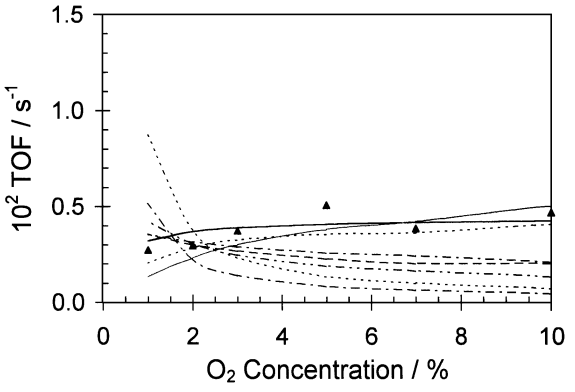

FIG. 9. Attempts at fitting various models to the experimental data for the effect of O_2 concentration on the rate of deNO_x; ▲, experimental points. Lines are fits to models given in Table 2: from top to bottom at 10% O_2, model 6, 8, 2, 5, 1, 4, 7, and 3; model 8 (the preferred model) is indicated by the bold line.

concentration is increased, the rate of C_3H_8 oxidation falls as a result of the decreased availability of vacant sites (see above), while the rate of the deNO_x reaction is enhanced (slightly). If vacant Pt sites were required for the deNO_x reaction then the rate would fall with increasing O_2 concentration. The reason for this mechanism not occurring may be that the high surface coverage of oxygen depresses the dissociation of NO and/or favours the reverse of reaction [16].

Attempts were made to correlate the rate of the deNO_x reaction to various combinations of surface coverages. However, the only correlation that was found was with the NO_2 coverage. That is the rate of deNO_x was given by

$$r_{NO_x} = k_{NO_x}\theta_{NO_2}. \qquad [17]$$

This can be interpreted in terms of a mechanism in which the rate-determining step is the spillover of adsorbed NO_2 onto the Al_2O_3 support. This NO_2 then reacts with C_3H_8 derived species deposited on the support, possibly located close to or at the metal-support interface, to give N_2 and N_2O. The transfer of NO_2 to the support occurs predominantly via spillover rather than by gas phase transfer, since if the latter were the case then the rate of deNO_x would be proportional to the gas phase concentration of NO_2, which is not the case; e.g., the conversion of NO to NO_2 falls with increasing C_3H_8 concentration, while the rate of deNO_x remains about constant.

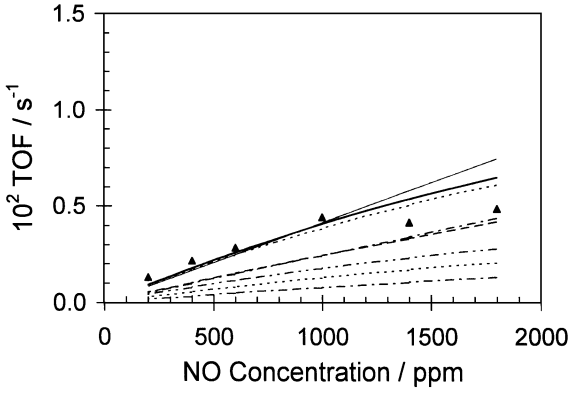

FIG. 8. Attempts at fitting various models to the experimental data for the effect of NO concentration on the rate of deNO_x; ▲, experimental points. Lines are fits to models given in Table 2: from top to bottom at 1800 ppm NO, models 8, 6, 2, 5, 1, 4, 7, and 3; model 8 (the preferred model) is indicated by the bold line.

This mechanism suggests that the nature of the support should be important, and indeed, while Pt/Al_2O_3 shows deNO_x activity with a C_3H_8–NO–O_2 feed, little (7, 16) or no (17) deNO_x activity is observed with Pt/SiO_2 with the same feed. Recently, Inaba and co-workers have reported that physical mixtures of Al_2O_3 and Pt/SiO_2 are active for deNO_x with a C_3H_8–NO–O_2 feed (17). This is consistent with the mechanism suggested above, although in this case the reaction presumably occurs by gas phase transfer of NO_2, produced by oxidation of NO on the Pt surface, to the surface of the Al_2O_3, where it reacts with C_3H_8 derived species. However, Inaba and co-workers rule this mechanism out on the basis that at lower temperatures (300–350°C) the NO_x conversion obtained with Al_2O_3 and a C_3H_8–NO_2–O_2 feed was less than obtained with a Pt/SiO_2 and Al_2O_3 physical mixture with a C_3H_8–NO–O_2 feed. This may be due to the Pt having another role in the deNO_x; for example, a partially oxygenated and/or oxidised intermediate derived from C_3H_8 may be more reactive with the Al_2O_3 than with C_3H_8.

The deNO_x reaction presumably occurs via NO_2, as opposed to NO because the former is much more reactive, both in general (18) and in particular for this sort of reaction; the deNO_x activity of Al_2O_3 is much greater with a C_3H_8–NO_2–O_2 feed than with C_3H_8–NO–O_2 (19). For many

deNO$_x$ catalysts with C_3H_8 as the reductant there is a general consensus that the first step in the deNO$_x$ reaction is the oxidation of NO to NO_2. A number of authors have suggested that this NO_2 then reacts with a reductant-derived species on the Al_2O_3 support. However, there is no consensus on how this happens in detail. Isocyanates have been detected on the Al_2O_3 supports and it has been suggested that these are reaction intermediates (20, 21) which react with NO to form N_2 and N_2O (15):

$$-NCO + NO \rightarrow N_2 + CO_2 \quad [18]$$

$$-NCO + NO \rightarrow N_2O + CO, \quad [19]$$

where −NCO represents an isocyanate group bonded to the support. The production of HCN, HNCO, and NH_3 by Al_2O_3 catalysts is also consistent with isocyanates being intermediates (22). Carbonaceous radicals have also been detected in the C_3H_6–NO−O_2 and *t*-butyl ether–NO−O_2 reactions on Al_2O_3 and the NO$_x$ conversion correlated to both the weight of carbon deposited and the spin density (independent of the hydrocarbon), suggesting that these carbonaceous radicals were reaction intermediates. Perhaps another possibility is that NO_2 reacts with the Al_2O_3 to form a nitrate species which is capable of reacting with the hydrocarbon. It is possible that the reaction occurs by a combination of some of these reactions, e.g., NO_2 reacts with a carbonaceous deposit to form an isocyanate species which reacts further to give N_2 and N_2O.

The fact that the rate of deNO$_x$ seem to depend only on the NO_2 coverage on the metal suggests that the concentration of C_3H_8-derived species with which the NO_2 reacts, is independent of reactant composition at this temperature. The literature on the C_3H_8–NO_2–O_2 reaction over Al_2O_3 was examined to see if this was reasonable. While no complete kinetic study appears to have been published, it is reported that changing the O_2 concentration from 1 to 10% had no effect on the NO$_x$ conversion (23). The lack of any composition dependence on the coverage of these C_3H_8-derived species on the support means that it is difficult to draw any further conclusions on how the NO_2 is converted to N_2 and N_2O.

It must be stressed that the mechanism proposed here is not universal for all deNO$_x$ catalysts and reductants. In particular, the kinetics of the propene–NO−O_2 reaction over the same catalyst used in this study were very different to those of the propane–NO−O_2 reaction, suggesting that the reaction mechanism is different (7, 24). With the former reaction, removal of NO most likely occurs by NO dissociation on reduced sites (i.e., reaction [16]) and does not involve the support.

The oxidation of C_3H_8 (or at least species derived from it) by NO_2 needs to be allowed for in the kinetic model for total C_3H_8 oxidation. The overall reactions of NO_2 and C_3H_8 to give N_2 and N_2O are

$$C_3H_8 + 5NO_2 \rightarrow 3CO_2 + 4H_2O + \tfrac{5}{2}N_2 \quad [20]$$

$$C_3H_8 + \tfrac{20}{3}NO_2 \rightarrow 3CO_2 + 4H_2O + \tfrac{10}{3}N_2O. \quad [21]$$

Thus the rate of reaction of C_3H_8 with NO_2 is given by

$$r_{C_3H_8\text{–}NO_2} = \frac{r_{NO_x}}{2000}(300 + S_{N_2}), \quad [22]$$

where S_{N_2} is the percentage selectivity to N_2, ignoring NO_2; i.e.,

$$S_{N_2} = \frac{100 n_{N_2}}{n_{N_2} + n_{N_2O}}, \quad [23]$$

where n_{N_2} and n_{N_2O} are the amounts of N_2 and N_2O formed. The fitted curves in Figs. 3–5 include both the C_3H_8–O_2 and C_3H_8–NO_2 reactions (Eqs. [12] and [22]).

Including the Effect of Temperature in the Kinetics Model

The kinetics model has been extended to include the effect of temperature by allowing for the variation in rate constants and adsorption coefficients with temperature and by allowing for the fact that at the higher conversions obtained at higher temperatures the reactor no longer behaves differentially.

The effect of temperature on the rate constants and adsorption coefficients was assumed to be given by the Arrhenius equation and Van't Hoff isochore, respectively; i.e.,

$$\ln\left(\frac{k_2}{k_1}\right) = -\frac{E_a}{R}\left(\frac{1}{T_2} - \frac{1}{T_1}\right) \quad [24]$$

$$\ln\left(\frac{K_2}{K_1}\right) = -\frac{\Delta H^{\ominus}_{ads}}{R}\left(\frac{1}{T_2} - \frac{1}{T_1}\right), \quad [25]$$

where k_1 and k_2 and K_1 and K_2 are rate constants and adsorption coefficients at temperatures T_1 and T_2; T_1 and T_2 are thermodynamic temperatures; R is the molar gas constant, E_a is the activation energy for the appropriate reaction step, and $\Delta H^{\ominus}_{ads}$ is the standard enthalpy of adsorption of the appropriate molecule.

The reactor was assumed to exhibit plug flow and transport limitations were assumed to be negligible. The effect of nondifferential conditions was included by allowing for concentration gradients along the catalyst bed. To do this the catalyst bed was divided into 20 sections along the direction of gas flow. The change in concentration across each section was calculated assuming each section behaved differentially; i.e., the reaction rates in each section depend on the concentrations at the beginning of the section, which are equal to the concentrations at the end of the previous section. Increasing the number of sections had no effect on the C_3H_8 concentration profile calculated along the bed, even at 100% C_3H_8 conversion.

TABLE 3

Mass Balance Equations Used for Calculating Conversions

Species	Mass balance equation
C_3H_8	$\delta c_{C_3H_8} = -A(r_{C_3H_8-O_2} + r_{C_3H_8-NO_2})\delta t$ [a]
NO	$\delta c_{NO} = -Ar_{NO_x}\delta t - \delta c_{NO_2}$ [b]
NO_2	$c_{NO_2} = \dfrac{k_{NO_2,f} c_{NO}\theta_O}{K_{NO_2} k_{NO_2,b}\theta_V}$ [c]
O_2	$\Delta c_{O_2} = 5 \times 10^{-4}\Delta c_{C_3H_8} - \dfrac{c_{NO_2}}{2 \times 10^4} - \dfrac{\Delta c_{NO_x}(S_{N_2} + 100)}{4 \times 10^6}$ [d]
CO_2	$\Delta c_{CO_2} = -3\Delta c_{C_3H_8}$
H_2O	$\Delta c_{H_2O} = -4\Delta c_{C_3H_8}$
N_2	$\Delta c_{N_2} = -\dfrac{\Delta c_{NO_x} S_{N_2}}{200}$
N_2O	$\Delta c_{N_2O} = -\dfrac{\Delta c_{NO_x}(100 - S_{N_2})}{200}$

Note. The catalyst bed was divided into sections (see text). δc_i is the change in concentration of i across the section, δt the time taken for a gas molecule to cross the section, Δc_i is the change in concentration of i between the reactor inlet and a given point in the catalyst bed, S_{N_2} the selectivity to N_2, ignoring NO_2 (Eq. [23]) and A is a constant to convert from TOF to rate in ppm s^{-1}.

[a] $r_{C_3H_8-O_2}$ and $r_{C_3H_8-NO_2}$ are given by Eqs. [12] and [22], respectively.

[b] r_{NO_x} is given by Eq. [17].

[c] Equation [15].

[d] Factors of 10^4 are to convert between % and ppm. The final term is to allow for the fact that some C_3H_8 reacts with NO_2 rather that O_2.

The conversion of NO to NO_2 and of NO_2 to NO is believed to be faster than the other reactions occurring on the catalyst, since the conversion to NO_2 was observed to be independent of contact time (Fig. 2). The concentration of NO_2 in each of the sections of the reactor was calculated using Eq. [15]. However, it was found that if the ratio of NO to NO_2 at the beginning of the catalyst bed was greatly different from the final concentration then the NO_2 concentration calculated along the bed exhibited damped oscillations. Changing the initial ratio of NO to NO_2 (at constant NO_x concentration) had little effect on the calculated C_3H_8 conversion and on the conversion to NO_2, but it did affect the calculated NO_x conversion since the rate of the deNO_x reaction is directly proportional to the NO_2 coverage, which in turn depends on the gas phase NO_2 concentration. This problem was solved by setting the ratio of NO to NO_2 at the beginning of the bed to be equal to that experimentally observed.

Conversions were calculated from the model using Microsoft Excel 5.0 and the mass balance equations listed in Table 3. The parameters given in Table 1 were determined by varying the parameters to minimise the sum of the square of the differences between experimental and calculated conversions using the Solver command in Excel.

This model was found to successfully fit the observed effect of temperature on the conversion of C_3H_8 and on the conversion to NO_2 (Fig. 1), but it did not predict the maximum in the NO_x conversion. The parameters are given in Table 1. Note that the activation energies are all positive while the heats of adsorption are negative as expected. A possible reason for the maximum in the NO_x conversion is that the concentration of the C_3H_8 species on the surface of the support with which the NO_2 reacts to give N_2 and N_2O decreases with temperature, possibly as a result of increased activity of the Al_2O_3 for C_3H_8 oxidation by O_2 with increased temperature, coupled with the fact that the C_3H_8 concentration falls with increasing temperature as a result of the increase in C_3H_8 conversion. Modification of Eq. [17] to include a term which allows for the fall in C_3H_8 derived species on the support with increasing temperature should enable the prediction of the maximum in NO_x conversion. However, in the absence of any further information on the mechanism of the NO_x reaction, any such modification of the rate expression could be based only on speculation.

It is notable that the values obtained for K_{NO} and K_{NO_2} and their temperature dependencies (Table 1) are, unexpectedly, practically the same. However, no significance should be attached to this, as alternative sets of parameters were also found to fit the empirical data. For example, the effect of temperature can equally well be fitted with the temperature parameters of K_{NO}, K_{NO_2}, k_{NO_x}, and $k_{NO_2,f}/k_{NO_2,b}$ set to -38.7, -65.9, 123, and -103 kJ mol^{-1}, respectively. Similarly, the concentration dependencies can be fitted with K_{NO} and K_{NO_2} set to 1.34×10^{-2} and 1.87×10^{-2} ppm^{-1}, provided the other parameters are also changed.

CONCLUSIONS

The effect of temperature, contact time, and reactant concentration on the kinetics of NO reduction by C_3H_8 under lean-burn conditions has been investigated and a kinetic model which satisfactorily fits the data has been developed. The proposed mechanism is summarised in Fig. 10.

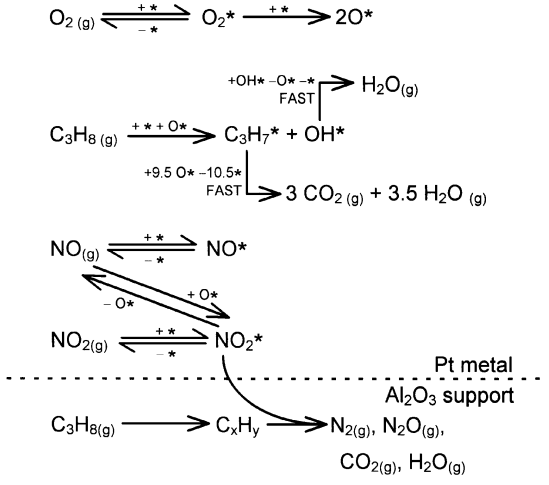

FIG. 10. Proposed mechanism for the C_3H_8–NO–O_2 reaction. Reactions above the dotted line occur on the Pt surface, while reactions below the line occur on the Al_2O_3 support.

Under reaction conditions adsorbed oxygen is the dominant species on the metal surface. This leads to inhibition of C_3H_8 oxidation by O_2 and the oxidation of NO to NO_2. Dissociation of NO does not seem to occur to any great extent on the metal. Instead, reduction of NO to N_2 and N_2O appears to occur by a mechanism involving spillover of NO_2 from the metal onto the Al_2O_3 support where it reacts with some C_3H_8 derived species, although the detailed mechanism of this reaction is unclear at present.

This mechanism suggests ways in which the deNO$_x$ activity of the catalyst could be improved. The deNO$_x$ reaction may be enhanced by modifying the support to better facilitate the reaction between NO_2 and C_3H_8 derived species, perhaps by adding a basic component to trap NO_2 or to aid C_3H_8 activation on the support (although not to the extent that the coverage of C_3H_8 derived species is reduced by the enhanced rate of reaction with O_2). Lowering the temperature of C_3H_8 activation by the support so that it coincides with the maximum in NO_2 production may also be beneficial.

APPENDIX 1: DERIVATION OF EXPRESSIONS FOR θ_V AND θ_O

In this appendix the derivation of the expressions for θ_V and θ_O (Eqs. [10] and [11]) are given in more detail than the main text.

Substituting Eqs. [6] and [7] into Eq. [9] and assuming θ_{O_2} to be negligible gives

$$\theta_O = 1 - \theta_V(1 + K_{NO}c_{NO} + K_{NO_2}c_{NO_2}). \quad [26]$$

Substituting this into Eq. [8] and dividing both sides by $10\theta_V$ gives

$$k_{OX}c_{O_2}(\theta_{O,MAX} - 1 + \theta_V)/5 = k_{C_3H_8}c_{C_3H_8}(1 - \theta_V(1 + K_{NO}c_{NO} + K_{NO_2}c_{NO_2})). \quad [27]$$

Solving this for θ_V gives

$$\theta_V(k_{C_3H_8}c_{C_3H_8}(1 + K_{NO}c_{NO} + K_{NO_2}c_{NO_2}) + k_{OX}c_{O_2}/5) = k_{C_3H_8}c_{C_3H_8} + k_{OX}c_{O_2}(1 - \theta_{O,MAX})/5 \quad [28]$$

$$\theta_V = \frac{k_{C_3H_8}c_{C_3H_8} + k_{OX}c_{O_2}(1 - \theta_{O,MAX})/5}{k_{C_3H_8}c_{C_3H_8}(1 + K_{NO}c_{NO} + K_{NO_2}c_{NO_2}) + k_{OX}c_{O_2}/5}. \quad [10]$$

Substituting Eq. [10] into Eq. [26] gives an expression for θ_O,

$$\theta_O = 1 - \frac{k_{C_3H_8}c_{C_3H_8} + k_{OX}c_{O_2}(1 - \theta_{O,MAX})/5}{k_{C_3H_8}c_{C_3H_8}(1 + K_{NO}c_{NO} + K_{NO_2}c_{NO_2}) + k_{OX}c_{O_2}/5} \times (1 + K_{NO}c_{NO} + K_{NO_2}c_{NO_2}). \quad [29]$$

$$\theta_O = \frac{k_{OX}c_{O_2}(1 - (1 - \theta_{O,MAX})(1 + K_{NO}c_{NO} + K_{NO_2}c_{NO_2}))}{5(k_{C_3H_8}c_{C_3H_8}(1 + K_{NO}c_{NO} + K_{NO_2}c_{NO_2}) + k_{OX}c_{O_2}/5)}. \quad [30]$$

$$\theta_O = \frac{k_{OX}c_{O_2}(\theta_{O,MAX} - (K_{NO}c_{NO} + K_{NO_2}c_{NO_2})(1 - \theta_{O,MAX}))}{5(k_{C_3H_8}c_{C_3H_8}(1 + K_{NO}c_{NO} + K_{NO_2}c_{NO_2}) + K_{OX}c_{O_2}/5)}. \quad [11]$$

APPENDIX 2: DERIVATION OF DENO$_x$ RATE BY REACTION OF NO$_x$ WITH CARBONACEOUS SPECIES

If the rate-determining step of the deNO$_x$ reaction is reaction between NO or NO_2 and a C_3H_8 derived species on the Pt surface then the rate of deNO$_x$ is given by

$$r_{NO_x} = k_{NO_x}\theta_{NO_x}\theta_C, \quad [31]$$

where θ_{NO_x} is the coverage of NO or NO_2 and θ_C is the coverage of the carbonaceous species involved. This reaction may occur via organo-nitrogen compound(s) or isocyanates as intermediates. Alternatively, the reaction may involve NO dissociation which is assisted by a carbonaceous species; i.e.,

$$NO* + C_xH_yO_z* \rightarrow N* + C_xH_yO_{z+1}*, \quad [32]$$

were $C_xH_yO_z*$ is a carbonaceous species, which could be oxygenated.

An expression for θ_C can be derived by consideration of mechanism of C_3H_8 oxidation and use of the stationary state approximation. A carbonaceous species on the Pt surface may either dissociate or react with an adsorbed oxygen atom, i.e.,

$$C_xH_yO_z* + * \rightarrow C_aH_bO_c* + C_{x-a}H_{y-b}O_{z-c}*, \quad k_1\theta_C\theta_V, \quad [33]$$

$$C_xH_yO_z* + O* \rightarrow C_xH_yO_{z+1}* + *, \quad k_2\theta_C\theta_O, \quad [34]$$

$$C_xH_yO_z* + O* \rightarrow C_xH_{y-1}O_z* + OH*, \quad k_3\theta_C\theta_O. \quad [35]$$

There are other possibilities for the reaction of carbonaceous species with adsorbed O. Assuming that these steps are irreversible, then, according to the steady state approximation, the rates of these steps are equal to the rate of C_3H_8 oxidation. Thus it follows that

$$\theta_C \propto \frac{r_{C_3H_8}}{\theta_V} \quad \text{or} \quad \frac{r_{C_3H_8}}{\theta_O}. \quad [36]$$

Since the amount of oxygen from O_2 reacting with C_3H_8 is an order of magnitude greater than that from NO, the reaction of NO and/or NO_2 with C_3H_8 can be ignored when calculating θ_C.

ACKNOWLEDGMENTS

We are grateful to the EPSRC for financial support for this work through Grant GR/K01452. We thank Johnson Matthey PLC for the supply of Pt salts.

REFERENCES

1. Burch, R. (Ed.), *Catal. Today* **26**, (1995).
2. Iwamoto, M. (Ed.), *Catal. Today* **22**, (1994).
3. Obuchi, A., Ohi, A., Nakamura, M., Ogata, A., Mizuno, K., and Ohuchi, H., *Appl. Catal. B* **2**, 71 (1993).
4. Zhang, G., Yamaguchi, T., Kawakami, H., and Suzuki, T., *Appl. Catal. B* **1**, L15 (1992).
5. Burch, R., and Watling, T. C., *Catal. Lett.* **37**, 51 (1996).
6. Burch, R., Millington, P. J., and Walker, A. P., *Appl. Catal. B* **4**, 65 (1994).
7. Burch, R., and Watling, T. C., *Catal. Lett.* **43**, 19 (1997).
8. Engler, B. H., Leyrer, J., Fox, E. S., and Ostgathe, K., "Catalyst and Automotive Pollution Control III" (A. Frennet and J-M. Bastin, Eds.), Stud. Surf. Sci. Catal., Vol. 96, p. 529, Elsevier, Amsterdam, 1995.
9. Yao, Y-F. Y., *Indus. Eng. Prod. Res. Dev.* **19**, 293 (1980).
10. Burch, R., and Hayes, M. J., *J. Mol. Catal. A* **100**, 13 (1995).
11. Burch, R., Urbano, F. J., and Loader, P. K., *Catal. Today* **27**, 243 (1996).
12. Engel, T., and Ertl, G., *Adv. Catal.* **28**, 1 (1979).
13. Huinink, J., Ph.D. thesis, Chap. 5, Technical University of Eindhoven, The Netherlands, 1995.
14. Tanka, T., Okuhara, T., and Misono, M., *Appl. Catal. B* **4**, L1 (1994).
15. Bamwenda, G. R., Obuchi, A., Ogata, A., and Mizuno, K., *Chem. Lett.* **1994**, 2109 (1994).
16. Millington, P. J., Ph.D. thesis, Chap. 5, University of Reading, U.K., 1995.
17. Inaba, M., Kintaichi, Y., and Hamada, H., *Catal. Lett.* **36**, 223 (1996).
18. Cotton, F. A., and Wilkinson, G., "Advance Inorganic Chemistry," 3rd ed., p. 354, Interscience, New York, 1972.
19. Hamada, H., *Catal. Today* **22**, 21 (1994).
20. Ukisu, Y., Miyadera, T., Abe, A., and Yoshida, K., *Catal. Lett.* **39**, 265 (1996).
21. Ukisu, Y., Sato, S., Muramatsu, G., and Yoshida, K., *Catal. Lett.* **11**, 177 (1991).
22. Radtke, F., Köppel, R. A., and Baiker, A., *Catal. Today* **26**, 159 (1995).
23. Hamada, H., Kintaichi, Y., Tabata, M., Sasaki, M., and Ito, T., *Sekiyu Gakkaishi* **36**, 149 (1993).
24. Burch, R., and Watling, T. C., unpublished results.